Astron. Astrophys. 266, 365–376 (1992)

ASTRONOMY AND ASTROPHYSICS

Sub-millimetre molecular lines in the circumstellar envelope IRC+10216

Peter G. Williams and Glenn J. White

Physics Department, Queen Mary & Westfield College, University of London, Mile End Road, London E1 4NS, United Kingdom
PGW @UK.AC.QMW.STAR.

Received March 21, accepted August 31, 1992

Abstract. Observations are presented of the circumstellar envelope IRC+10216 obtained with the 15m James Clerk Maxwell Telescope . Maps with the 15″ FWHM beam have been made in the CO $J=3-2$, CS $J=7-6$ and HCN $J=4-3$ transitions. The shape of the radial CO distribution agrees well with the Kwan-Linke outflow model. The HCN $J=4-3$ intensity is significantly greater than that of CO $J=3-2$, but drops off almost twice as rapidly with distance from the source centre. This rapid fall-off of the HCN intensity is indicative of the dominance of radiative excitation, which contrasts with the mainly collisional mechanism driving CO excitation. Single spectra at or near the source centre are also presented for the isotopes ^{13}CO, H^{13}CN, C^{34}S, for the $J=3-2$ line of HCN and its isotope H^{13}CN (with 23″ FWHM beam) and for CO $J=4-3$ (11″ FWHM beam). Upper limits are also obtained for the C^{18}O $J=3-2$ isotopic line and for the neutral carbon $^3P_1$–$^3P_0$ fine structure transition at 492.16 GHz. Simple modelling leads to estimates of relative abundances and excitation temperatures of CO, HCN and CS and an upper limit to the neutral carbon abundance.

Key words: radio lines: molecular – stars: circumstellar matter, late-type, carbon, mass loss

1. Introduction

Of the approximately 125 known Carbon-rich circumstellar envelopes, IRC+10216 is by far the brightest and most intensively studied. First discovered at 2μm (Neugebauer & Leighton 1969; Becklin et al. 1969), this outflowing molecular envelope surrounding a carbon-rich Mira variable embedded in a dust shell, has been mapped in both CO $J=1-0$ and $J=2-1$ rotational lines out to a radial distance of 240″ (Huggins et al. 1988) corresponding to some 70,000 AU at a distance of 290 pc. The dust has been mapped in reflection out to 60″ (Tamura et al. 1988); the observed continuum spectrum, ranging from 0.5 to 3000μm and peaking at 10μm, may be understood as arising from an underlying $L \approx 10^4 L_\odot$, 2000 K stellar Planck spectrum processed by a surrounding amorphous carbon dust envelope (Martin & Rogers 1987 and references therein; Orofino 1990). There is some evidence that this dust-dominated region can be modelled as a two-component structure consisting of an inner hot 600 K blackbody core 0.″2 in radius (Toombs et al. 1972) surrounded by a cooler 375 K dust envelope extending out to 1.″0 (Foy et al. 1979). Recent observations at 3.4μm (Bloemhof et al. 1988) are consistent with this picture but indicate that the two components do not have sharp boundaries (Sutton et al. 1979).

A rich Carbon chemistry arises from high threshold reactions occuring in the hotter inner regions producing molecules which then flow outwards while cooling to the point where the abundances created in near LTE conditions "freeze out" (McCabe et al. 1979). Without further processing the major part of the molecular envelope would be expected to exhibit constant composition beyond the "freeze out" radius: however the interstellar radiation field and cosmic rays are expected (Huggins & Glassgold 1982) to have a marked effect on the composition via photodissociation reactions, leading to the destruction of CO, HCN, C_2H_2, NH_3 and the formation through ion-molecule chemistry of other new species. Because all molecules are destroyed in the outermost regions exposed to the full interstellar UV field, the expectation is of a complex shell-like structure in molecular species created in this manner (Lafont et al. 1982; Glassold et al. 1986; Nejad & Millar 1987; Truong-Bach et al. 1987). Both these effects appear to have been established by recent observations: in their extensive mapping beyond a radius of 60″ in CO $J=1-0$ and $J=2-1$ Huggins et al. (1988) have found large deviations from the standard model without external heating, good fits being achieved with CO depletion by the UV field ; while Bieging & Nguyen-Q-Rieu (1988) have found evidence for shell structure in the ion-molecule chemistry products HNC and C_2H.

IRC+10216 is a unique source of astrophysical information from several points of view: its comparative proximity has made it possible to detect some 30 or more molecular species (see Olofsson 1988 for a recent review) and study its structure and dynamics in great detail, while its near spherical symmetry makes it an ideal subject for reliable theoretical modelling. As an evolved star shedding its mass it is the prototype for one of the two main sources of enrichment for the interstellar medium, the other being supernovae. Finally, it is likely that IRC+10216 is a planetary nebula in its early superwind stage, and that a detailed study of the dynamics of the outflow may yield unique information on the history of mass loss during this important phase of the life of such stars (Sahai 1987). Although IRC+10216 has been subject to extensive study over the last 20 years since its discovery, there is surprisingly little quantitatively reliable data, and a need

Send offprint requests to: P.G. Williams

for more theoretical modelling, particularly of molecular lines other than CO (see, however, Nguyen-Q-Rieu 1984; Morris et al. 1985; Sahai 1987 and Truong-Bach et al. 1989). This contrasts markedly with the situation regarding infrared observations and the properties of the dust envelope, where a consensus now exists: predominantly amorphous carbon dust provides an excellent fit over the entire range 0.5 - 1000μm (Rowan-Robinson et al. 1986; Martin & Rogers 1987; Orofino et al. 1990). Indeed, a study of the nature of this dust yields uniquely precise information on interstellar dust in general.

In Sects. 2 and 3 we present data covering the submillimeter region between 250 and 461 GHz, including maps in CO $J=3$–2, CS $J=7-6$ and HCN $J=4-3$, as well as single spectra taken at or near the source centre of HCN $J=3-2$, CO $J=4-3$ and the isotopic species ^{13}CO, C^{34}S and H^{13}CN. We have also set 1 σ upper limits on the strengths of the $J=3-2$ C^{18}O and neutral carbon $^3P_1$–$^3P_0$ fine structure lines. In Sect. 4 we discuss the source profiles in CO $J=3$–2, CS $J=7$–6 and HCN $J=4$–3, giving model fits to the CO profile and phenomenological fits to CS and HCN for comparison. A simple outflow model enables us to estimate the relative abundances of CO, CS and HCN.

2. Observations

The observations were carried out during February and July 1988 (CO $J=4$–3 in December 1991) using the 15-m JCMT telescope situated on Mauna Kea, Hawaii [1]. The telescope was operated in position switched mode with an off-source throw of 10′; all data was taken with repeated integrations 10 seconds on-source followed by 10 seconds off-source. Intensities were output and stored as antenna temperature T_A^*, calibrated at regular intervals by means of a hot and cold load, and corrected for atmospheric absorption; dividing by η_{MB} (Table 1) then gives the main beam brightness temperature T_{MB}, the quantity most commonly used in work on circumstellar envelopes. T_{MB} is the quantity to be compared with our theoretical modelling where we convolve a model radiation temperature distribution $T_R(r)$ with a Gaussian main beam (see Eq. (6)). For this frequency regime the JCMT beam is well modelled by a single Gaussian.

For our measurements we used three heterodyne receivers, each with a cryogenically cooled Schottky diode detector feeding an acousto-optical spectrometer (AOS). Relevant measured parameters are listed in Table 1. At frequencies in the range 330-355 GHz (Receiver B) we operated with a bandwidth of 500 MHz in 1024 oversampled channels giving an effective velocity resolution of 0.85 km s^{-1}. The total system noise temperature ranged between 2500-3000 K (DSB) depending on frequency, elevation and atmospheric conditions. For calibration of the lines we have assumed equal gain in each of the two sidebands, confirmed by subsequent tests of the receiver sideband ratios to within 10–20%. For the HCN $J=3-2$ spectra in the lower frequency regime (Receiver A), the velocity resolution was 1.15 km s^{-1} with the system noise temperature considerably lower at 1000-2000 K. The high frequency measurement of the CI line at 492 GHz with Receiver C gave similar noise temperatures, with a velocity resolution of 1.0 km s^{-1}. All instrumental baselines were removed by fitting with low order polynomials determined from empty channels away from the spectral lines. The RMS noise level in channels just off the spectral lines was typically 1-2 K for the higher frequency measurements as expected for the level of system noise and integration times; but for the HCN $J=3$–2 spectra this fell to $\sim$ 0.2 K.

Telescope pointing, frequently checked by reference to Mars or Jupiter, was estimated to be accurate to within 5″– 10″ during February, when most of the CO and CS maps were made; but by July, when the HCN maps were taken and a consistency check on the CO peak temperature made, the pointing had improved to 2″– 3″. Tracking accuracy appeared to be better than 1″ over periods of an hour.

Table 1. Receiver & telescope parameters

Receiver/FWHM	Measurement	Measured Efficiencies.	
		η_{fss}	η_{MB}
Rec.A/23″	Jan.88-Jun.88	0.7 ± 0.1	0.55 ± 0.05
	Jul.88-Oct.89[a]		0.60 ± 0.03
Rec.B/15″	Sep.87-Dec.87		0.43 ± 0.10
	Jan.88-Jun.88[b]	0.8 ± 0.1	
	Jul.88-Oct.89		0.55 ± 0.10
Rec.C/11″	Nov./Dec. 1991[c]		0.39 ± 0.05

[a] HCN $J=3-2$ & H^{13}CN $J=3-2$ data taken on 14-16 Oct.88.
[b] CO & ^{13}CO $J=3$–2, CS & C^{34}S $J=7-6$ data taken on 20-26 Feb.88.; CO confirmed 26 Jul.88.
[c] CO $J=4-3$ data taken Dec.91.

3. Results

3.1. Maps and radial profiles

One of the most useful measurements for any detailed modelling of IRC+10216 is the acquisition of reliable maps in the species to be studied. This is especially so for the higher excitation lines presented here because the rapid radial decrease in these line strengths, combined with any errors in telescope pointing can lead to serious underestimates of peak temperatures; a map makes it possible to subsequently determine the source centre and hence to carry out any necessary interpolation. We have made several maps in CO $J=3-2$, CS $J=7-6$ and HCN $J=4-3$ some of which are displayed in Figs. 1, 2 and 3. The CO and CS spectra were obtained simultaneously, with CS in the lower side-band of the receiver.

The maps indicate that IRC+10216 is *approximately* spherically symmetric in these lines, at least within the uncertainties introduced by possible tracking errors, baseline subtraction and beam shape. In each of our maps, including the ones not shown here, we determined the central point of the source from the average of the middle of the highest few contours, thereby obviating any dependence on the less reliable *absolute* pointing accuracy. Hence, ignoring deviations from spherical symmetry, we are able to derive the line-of-sight distance p_0, in arcsec, of each mapped position from this self-consistently determined centre point. This leads to the source profiles given in Figs. 4, 5 and 6, which can be used for comparison with spherically symmetric outflow models.

[1] The James Clerk Maxwell Telescope is operated by the Royal Observatory Edinburgh on behalf of the Science and Engineering Research Council of the United Kingdom, the Netherlands Organisation for Scientific Research and the National Research Council of Canada.

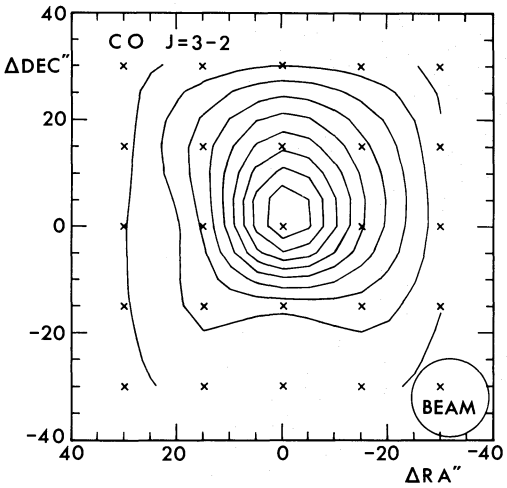

Fig. 1. Map of integrated T_A^* for CO $J = 3-2$, with integration limits -40 and -10 km/s. Data positions, marked by crosses, are 15″ apart. Contours are 30 K km/s apart, the lowest shown is at 30 K km/s; the highest at 270 K km/s

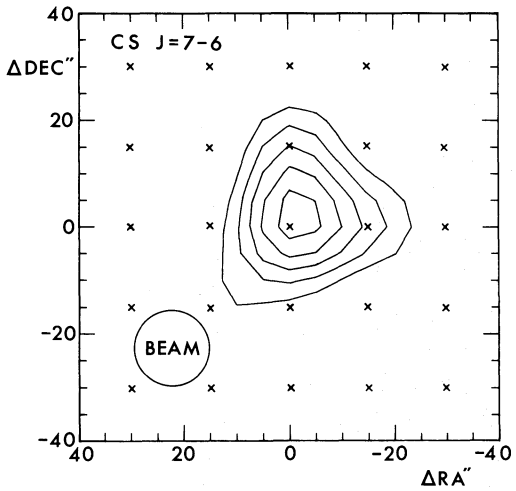

Fig. 2. Map of integrated T_A^* for CS $J = 7-6$. Contours are 15 K km/s apart, the lowest shown is at 30 K km/s; the highest at 90 K km/s

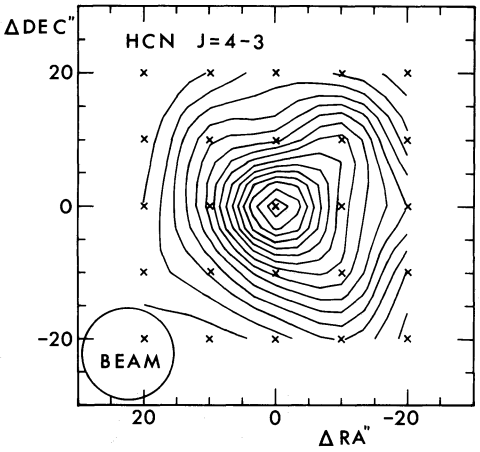

Fig. 3. Map of integrated T_A^* for HCN $J = 4-3$. Data positions are at 10″ spacing. Contours are 40 K km/s apart, the lowest shown is at 20 K km/s; the highest at 580 K km/s

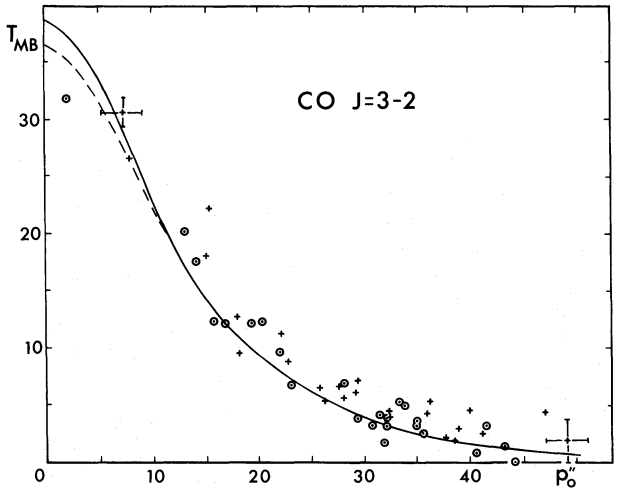

Fig. 4. Profile of IRC+10216 in CO $J = 3-2$ derived from two separate maps, denoted by different symbols. Typical error bars are shown for only two points at either extremity. The displacement of each mapped point from the source centre, p_0, was obtained by using the centre point derived from the contour plots, and should therefore not depend strongly on absolute pointing errors. Solid curve is the K-L model prediction for a 15″ FWHM beam; dashed curve for a 14″ FWHM, *both scaled* to achieve a best fit. T_{MB} is obtained with $\eta_{MB} = 0.43$

We note that for neither of the four CO nor CS maps did we actually hit the source centre: the best we achieved was some 2″ off-centre. In Sect. 4 we use our model fits to obtain an extrapolation to source centre. A major part of the scatter in Figs. 4 and 5 and the large error bars in Fig. 6 are probably due to the asymmetries evident in our contour maps, although below 1 or 2 K it is the low signal/noise level which is dominant.

All the maps, whether for integrated line profiles or peak temperature, consistently show a steeper falloff in the southern hemisphere than the northern, a result also hinted at in the high spatial resolution 9″ FWHM map in HCN $J = 1-0$ made with the Hat Creek interferometer (Bieging et al. 1984). This at least suggests that the inner regions of the gas envelope probed by the high excitation molecular lines presented here may not be spherical; but it would demand much more detailed oversampled mapping, as well as a thorough study of the beam shape, to establish this result convincingly. Recent mapping in the CO $J = 6-5$ line at the JCMT (Sahai et al. 1990) reveals strong asymmetries, suggesting that the inner molecular outflow is indeed not spherical. Lack of spherical symmetry of the outer dust shell (~ 5″) is evident in the original optical continuum (0.5-0.7μm) image of Becklin et al. (1969), showing an ellipsoidal shape with its major axis nearly along the E-W axis; this elongation is also seen in the inner shell (~0.5″) between 2.2-5μm (McCarthy et al. 1980), while high quality CCD imaging at ~0.9μm (Le Bertre 1988; Williams & Phillips, 1990) reveals a complicated triangular profile with the base lying NE-SW and the apex towards the SE. This asymmetry of the stellar flux provides a natural explanation for the unexpectedly high dust emission for wavelengths below 1 μm (Orofino et al. 1990) and for the existence of CN absorption bands (Miller 1970; Le Bertre 1988). For a discussion and further

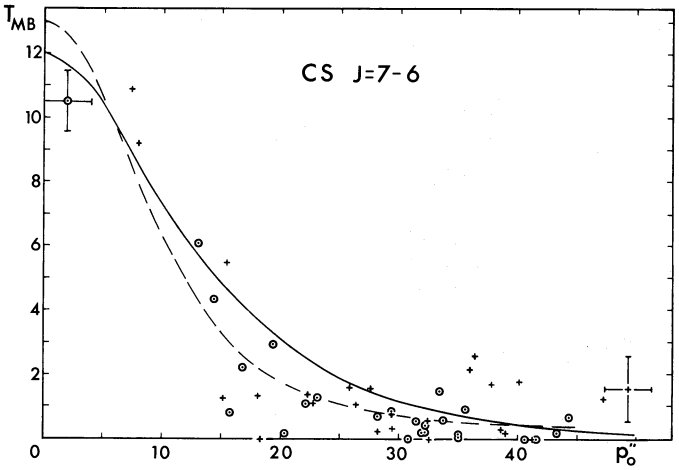

Fig. 5. Profile of IRC+10216 in CS $J = 7-6$; notation as in Fig 1. The solid curve is the K-L model prediction for CO $J = 3-2$, convolved with the 14″ beam; the dashed curve is the HCN fit shown in Fig. 6; both are rescaled to achieve a best fit

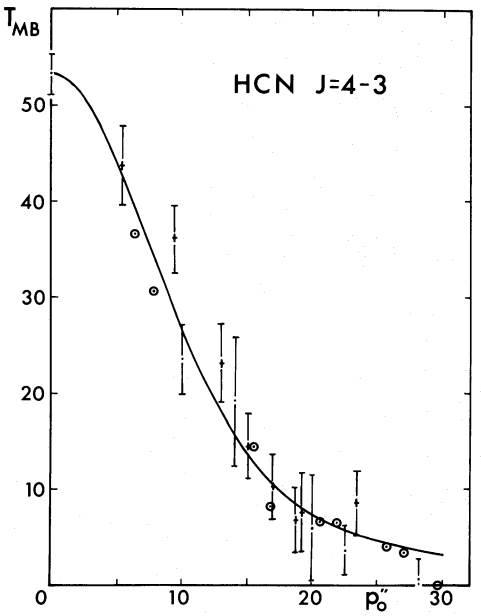

Fig. 6. Profile of IRC+10216 in HCN $J = 4-3$ for three separate maps, denoted by different symbols. Each point represents an average of several mapped points equidistant from the source centre, whose scatter dominates the error bars shown. Points without error bars have errors comparable to neighbouring points. The solid curve is a $1/p_0^{0.7}$ distribution convolved with the JCMT's 14″ FWHM beam. The convolved K-L model for CO $J = 3-2$, raised to the power 1.7 and rescaled fits the data equally well, and is indistinguishable from the fit shown out to 10″

references, see Martin & Rogers (1987).

3.2. *Spectra*

The CO $J = 3-2$ and $J = 4-3$ spectra, Figs. 7 & 15, are well fitted by the parabolic shapes typical of a resolved optically thick envelope with constant outflow velocity $(15 \pm 1)\,\mathrm{km\,s^{-1}}$ and $1/r^2$ density distribution (Morris 1975; Kuiper et al. 1976); similarly the ^{13}CO $J = 3-2$ line shown in Fig. 8 is optically thin, displaying either a flat top or a weak central dip and a full width at zero power (FWZP) consistent with the same outflow velocity. The absence of a marked central dip may be due to optical thickness in the line horns or to mispointing. If the ^{13}CO $J = 3-2$ falloff with distance from the source centre is anything like that of $J = 1-0$ (see the ^{13}CO map in Mauersberger et al. 1989) then the mispointing would have to be at least as large as 20″; but we expect the $J = 3-2$ falloff to be faster than $J = 1-0$, and our modelling indicates that the observed weak central dip can be reproduced by a 5″ pointing error. We also integrated on the C^{18}O, $J = 3-2$ line, setting a 1σ upper limit of $T_{MB} < 0.7$ K per channel; similarly, integration on the CI $^3P_2$–$^3P_1$ fine structure line sets a 1σ upper limit of $T_{MB} < 1.5$ K per channel. The CS $J = 7-6$ line in Fig. 9 is again optically thick, while the optically thin C^{34}S $J = 7$–6 line in Fig. 10 shows no obvious sign of a central dip, although it would be hard to see with such a low signal-to-noise level; and it may also be disguised by poor pointing. The HCN, $J = 4-3$ spectra in Figs. 11 and 12 are not so simple to interpret: the HCN line, with the hint of a somewhat flattened top, may be saturated, and H^{13}CN shows none of the classic signs of being optically thin, although our modelling suggests that it is. However, the much more rapid fall-off seen for HCN in Fig. 6, nearly half the width of the CO profile, suggests that the source is not resolved in HCN $J = 4$–3, a result confirmed by our modelling in Sect. 4; thus we do not expect to see a central dip in the isotope, although it *is* optically thin. We also note that the HCN $J = 4-3$ line is the strongest in this submillimetre region, significantly stronger than CO $J = 3$–2; this may seem surprising at first sight when compared with the $J = 1-0$ CO and HCN lines in the Onsala beam which are very nearly the same strength (Olofsson et al. 1982). We can ascribe this almost entirely to the

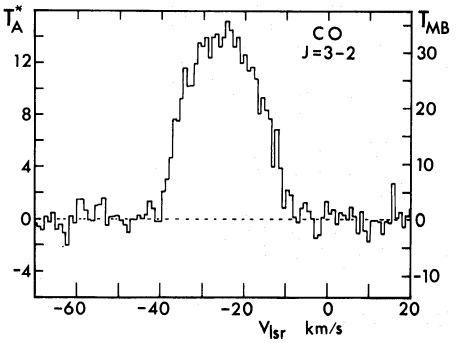

Fig. 7. CO $J = 3-2$ spectrum 2″ from source centre, as determined from the map in Fig. 1

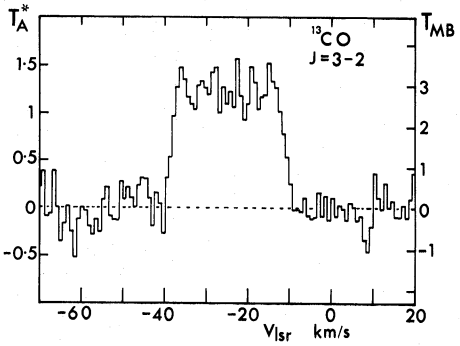

Fig. 8. ^{13}CO $J = 3-2$ spectrum at source centre ($\pm 5''$)

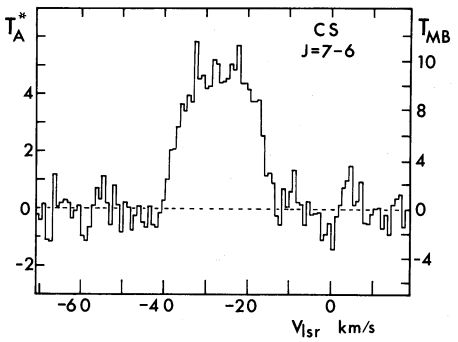

Fig. 9. CS $J = 7-6$ spectrum 2″ from source centre, as determined from the map in Fig. 2

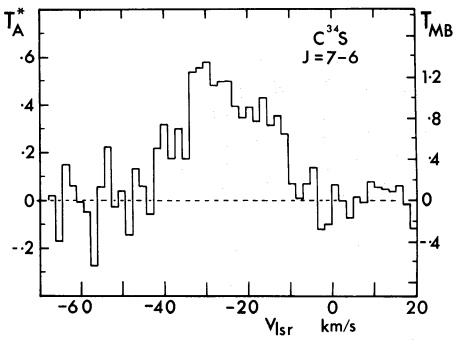

Fig. 10. $C^{34}S$ $J = 7-6$ spectrum at source centre ($\pm 5''$)

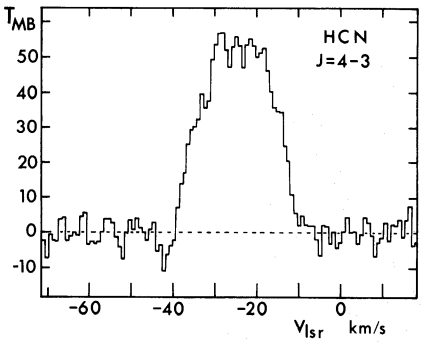

Fig. 11. HCN $J = 4-3$ spectrum at source centre, as determined from the map in Fig. 3

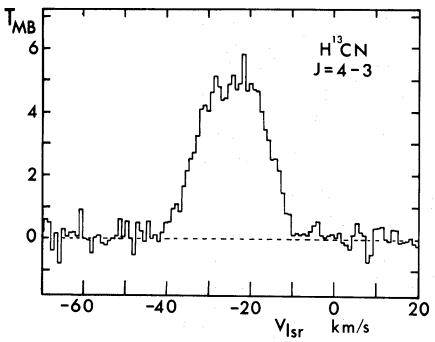

Fig. 12. $H^{13}CN$ $J=4-3$ spectrum at source centre ($\pm 5''$)

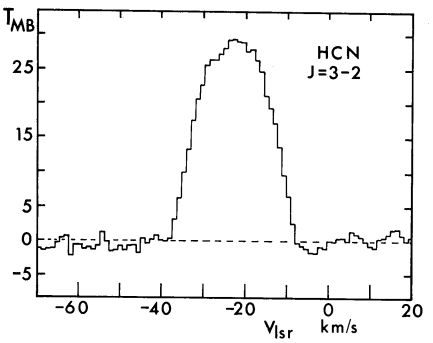

Fig. 13. HCN $J = 3-2$ spectrum at source centre ($\pm 5''$)

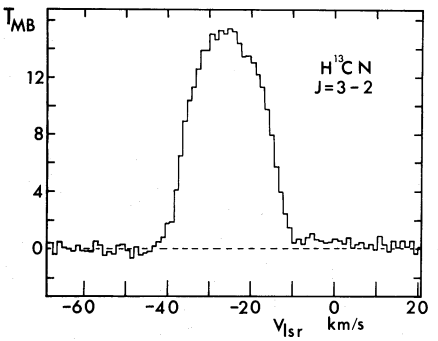

Fig. 14. $H^{13}CN$ $J=3-2$ spectrum at source centre ($\pm 5''$)

effects of beam dilution: on the basis of our simple modelling in Sect. 4 we estimate that the observed Onsala HCN(1-0)/CO(1-0) ratio of 1 would be measured as 1.7 in the smaller JCMT beam simply because the HCN radial distribution falls off so much faster than that of CO. Figures 13 and 14 show the HCN and $H^{13}CN$ $J=3-2$ spectra at source centre. These have a structure quite similar to the $J=4-3$ lines, again diplaying a significantly greater strength than the CO lines in the same excitation regime measured at the NRAO 12-m telescope (Huggins et al. 1988) after scaling to the narrower 23″ JCMT beam. The strength of the HCN lines relative to the collisionally excited CO points to the dominance of radiative excitation for the higher dipole moment HCN; a conclusion consistent with the faster radial falloff seen in HCN (Fig. 6): as we explore the higher excitation lines we are sampling regions closer in to the radiation source where the radiation field becomes more intense and has been less degraded by dust absorption; as we move outwards the radiation passes energy and momentum to the dust which re-emits in the IR and passes energy and momentum to the gas via collisions. The former is the dominant mechanism for exciting HCN – and probably CS; the latter for CO.

The strength of HCN in circumstellar envelopes has been noted before: in the carbon-rich AFL 2233 as well as IRC+10216, where HCN is found to be brighter than CO (Zuckerman & Dyck 1986; Nguyen-Q-Rieu et al. 1987); in oxygen rich circumstellar envelopes where it almost certainly results from processes which give rise to carbon in a form different from CO, and which is more abundant than that predicted by LTE chemistry (Nejad & Millar 1988; Nercessian et al. 1989). In carbon-rich envelopes the strength of HCN probably results from radiative rather than collisional excitation and may even lead to population inversion (Zuckerman 1986). Further evidence that radiation

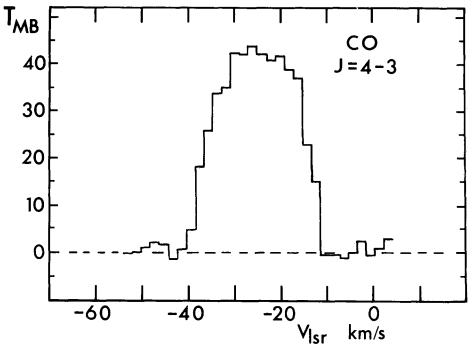

Fig. 15. CO $J = 4 - 3$ spectrum at source centre. The short baseline is due to the limited spectrometer bandwidth

is more efficient than collisional excitation for HCN emission comes from multilevel radiative transfer calculations (Truong-Bach & Nguyen-Q-Rieu 1989) which also show strong additional enhancement due to line overlap of hyperfine components. HCN maser-strength emission in the $(0,1^{1e},0)$ J=2-1 line has recently been observed at IRAM (Lucas & Cernicharo 1989).

The presence of turbulence causes small asymmetries in optically thick line profiles (Morris et al. 1985; Nguyen-Q-Rieu et al. 1984; Huggins & Healy 1986) shifting the peak towards the red, enhancing the red and depleting the blue half of the line and producing a slight toe feature on the blue wing. With high signal-to-noise spectra these diagnostics have provided a powerful method of measuring the systemic velocity (V_{lsr}), outflow velocity (V) and turbulent velocity width (ΔV at FWHM): for IRC+10216 Huggins & Healy (1986) obtained $V_{lsr} = -26.46 \pm 0.14\,\mathrm{km\ s^{-1}}$, $V = 14.1 \pm 0.15\,\mathrm{km\ s^{-1}}$ and $\Delta V = 0.9 \pm 0.15\,\mathrm{km\ s^{-1}}$. Although it is possible to see hints of all three features in some of our spectra the signal-to-noise level is too low to establish them with any confidence.

4. Modelling

In the present paper we have restricted the discussion to a comparison with the K-L model for the CO radial profile (Kwan & Hill 1977; Kwan & Linke 1982), phenomenological fits to the CS and HCN profiles as a comparison with CO, the application of a simple outflow model for estimating tangential optical depths, excitation temperatures and relative abundances (Morris 1975; Kuiper et al. 1976; Olofsson et al. 1982), and a comparison with other data.

4.1. The standard model

In the "standard" model of IRC+10216 (Kwan & Hill 1977; Morris 1980; Kwan & Linke 1982; Sahai 1987) the inner dust shell surrounding the carbon star acts as a 350 K near infrared continuum source with a Planck spectrum which drives the dust grains outwards by radiation pressure. These pass momentum to the gas via dust-gas collisions, producing a terminal outflow velocity $V = (15 \pm 1)\,\mathrm{km\,s^{-1}}$ through a balance between the radiation pressure and gas drag forces. As the outflow proceeds the gas, heated by collisions with the dust, cools mainly by adiabatic expansion and CO millimetre line emission. The balance between these three processes determines the run of kinetic temperature $T_{kin}(r)$ which forms the basis of subsequent radiative transfer calculations for the molecular lines of interest. Our present understanding of the molecular lines begins with the observation first made by Morris (1975) that the observed molecular intensities cannot be explained by collisional excitation alone because they require too large a density and hence an unreasonably large envelope mass. Instead the molecules are excited to higher *vibrational* states by the 2 - 20μm continuum radiation from the stellar and dust core; subsequent decay to the ground vibrational state then leaves a significant fraction of molecules in excited *rotational* states with $J \neq 0$; only for CO do collisions provide the dominant excitation mechanism. Of the important parameters of the model, V is set by the line widths (FWZP÷2), the luminosity L by infrared observations while the distance D, taken by K-L as 200 pc (Herbig & Zappala 1970) is uncertain to within a factor of about two. The remaining parameters, which are less well constrained, include the mass loss rate $\dot{M} = 4 \times 10^{-5} M_\odot\,\mathrm{yr^{-1}}$, abundance ratio $[\mathrm{CO}]/[\mathrm{H_2}] = 6 \times 10^{-4}$, dust-to-gas ratio, grain radius and density, and the efficiency for momentum transfer from grains to gas. The kinetic temperature distribution is well described by the power law fit:

$$T_{kin}(r) = 350 \left(\frac{0.384}{r''}\right)^{0.7} \mathrm{K} \tag{1}$$

with r'' the angular displacement in arcsec corresponding to the radial position r from the star centre for a distance of 200 pc. The K-L model has generally given a satisfactory account of the extant CO $J = 1 - 0$ and $2 - 1$ maps out to some 60″; beyond this radius the model decreases too rapidly. This failure has been attributed to gas heating and CO photodissociation in the outer envelope by the interstellar radiation field (Huggins et al. 1988; Mamon et al. 1988), providing a successful model fitting the large scale CO $J = 1 - 0$ distribution out to 200″.

Sahai (1987), arguing that the K-L model is not consistent with the higher kinetic temperature for the inner 2″ deduced from the CO 4.6μm IR lines (Sahai & Wannier 1985), has studied possible modifications to the K-L model. He finds that for the CO $J = 1 - 0$ and $J = 2 - 1$ lines it is possible to improve on the K-L fits to the line *shapes* by adopting a larger distance of 300 pc, with a slightly scaled down kinetic temperature (Knapp & Morris 1985) and a higher mass loss rate $\dot{M} = 4.8 \times 10^{-5} M_\odot$. With an increased central temperature this fine-tuned K-L model provides a considerably improved fit to the extant data.

4.2. Source profiles

The K-L model (Kwan & Linke 1982) provides a source radiation temperature distribution $T_R(p)$ in the plane of the sky at an angular offset p from the source centre; convolution with the normalised Gaussian beam,

$$P_n(p) = \frac{1}{\sigma^2} e^{-\pi p^2/\sigma^2} \tag{2}$$

(where the beam FWHM is $B = \sigma\sqrt{4 \ln 2/\pi}$) gives the main beam temperature $T_{MB}(p_0)$ observed by a telescope whose beam centre points towards a point p_0 off-centre

$$T_{MB}(p_0) = 2 \int_0^\infty p\,dp \int_0^\pi d\phi\, T_R(p) P_n(|p - p_0|) \tag{3}$$

where

$$|p - p_0|^2 = p^2 + p_0^2 - 2pp_0 \cos\phi \tag{4}$$

The two fits to CO $J=3-2$ in Fig. 4 show that the original K-L model for $T_R(p)$, convolved with a 14″–15″ JCMT beam, gives an an acceptable fit to the radial profile both in *shape* and, at the limits of our error bars, in *magnitude*. These fits provide a method of extrapolation for estimating the source centre temperature $T_{MB}(p_0 = 0)$, although the high resolution and sharply peaked source is responsible for considerable sensitivity to the rather imprecisely determined beam size. Thus the small uncertainty in FWHM, 14″–15″, compatible with the measured range over the first few months of JCMT operations, translates into an uncertainty of at least 1 K in the predicted central temperature. Furthermore, it is also possible to argue that the two measured points at 2″ and 5″ are consistent with a rather gentler approach to the centre than implied by the K-L model, leading to a lower central temperature. Another consequence of the high resolution is that beam dilution is only significant for the CO map within the inner 10″; further out, T_{MB} follows $T_R(p_0)$ rather closely. In our later discussion we take the success of these fits with the K-L model profile shape as justification for using their $T_R(p_0)$ (Kwan & Linke 1982; Fig. 3) as a good representation of the intrinsic CO $J=3-2$ radiation temperature profile, but not necessarily of the absolute intensity.

For CS and HCN we have attempted a comparison with CO by using the K-L model as a template for fitting their respective profiles. Empirical fits have been made to the CS and HCN profiles by convolving the JCMT beam with different powers of the K-L prediction for CO $J=3-2$ and searching for an acceptable fit: for CS the data is consistent with the CO profile itself (a power of 1, Fig. 5), although it may fall off faster beyond 15″ where the signal/noise level is too low to draw any firm conclusions; for HCN a good fit is obtained by using a power of 1.7; an equally acceptable fit to HCN is the one shown in Fig. 6 based on convolving the simple power law followed by the kinetic temperature:

$$T_R(p) = \begin{cases} 92.2\left(\frac{3.4}{p''}\right)^{0.7}\,\mathrm{K} & \text{for } p > 3.4'' \\ 92.2\,\mathrm{K} & \text{for } p \le 3.4'' \end{cases} \tag{5}$$

This fit is presented as a purely empirical one and has no obvious physical interpretatation; indeed it is rather surprising that the radiatively excited HCN should follow the run of kinetic temperature. For comparison we also show, in Fig. 5, how the more rapidly falling HCN profile compares with the CS data: clearly this is also an acceptable fit to the CS profile within the rather large error bars, although not as good as the K-L CO $J=3-2$ fit.

4.3. *Abundances and excitation temperatures*

In conjunction with the source profiles the isotopic data enables us to estimate optical depths, excitation temperatures and abundances. Ideally we should undertake a complete modelling of the level populations in non LTE conditions, taking account of the infrared pumping mechanism to enhance the population of higher J CO levels (Morris 1975; Morris & Alcock 1977), and using an escape probability formalism to calculate the radiative transfer. The resulting radiation temperature profile, $T_R(r)$, when inserted into Eq. (6) below would yield both spectra and source profiles to determine the unknown abundances by fitting our data. Leaving this as a task for the future we use instead a simpler LTE model of a constant radial outflow (Kuiper et al. 1976; Morris 1975; Olofsson et al. 1982), with velocity V, which should yield first order estimates. In this model the main beam temperature for a telescope pointing at an impact parameter p_0 and receiving at a frequency corresponding to a line-of-sight velocity $\beta = V_\parallel/V$ is given by a convolution integral of the Gaussian telescope beam and source:

$$\begin{aligned} T_{MB}(p_0,\beta) \;=\; & \frac{2\pi}{\sigma^2}(1-\beta^2)e^{-\pi p_0^2/\sigma^2}\int_{r_i}^{r_e} r\,dr \\ & T_R(r)\left(1-e^{-\tau_0\sigma/r(1-\beta^2)}\right)e^{-\pi r^2(1-\beta^2)/\sigma^2} \\ & I_0\left(\frac{2\pi}{\sigma^2}rp_0(1-\beta^2)^{\frac{1}{2}}\right) \end{aligned} \tag{6}$$

Integration over the source radial coordinate r ranges from an inner core radius r_i to an outer r_e while the zeroth-order Bessel function I_0 arises from the angular integration. The tangential optical depth, τ_0, is the optical depth at $\beta = 0$ and $r = \sigma$:

$$\begin{aligned} \tau_0 \;=\; & \frac{N_0 r_0^2}{\sigma}\left[\frac{A_{J,J-1}c^3}{8\pi\nu^3 V}(2J+1)\frac{e^{-hB_0J(J+1)/kT_{ex}}}{Z}\right. \\ & \left.\left(e^{h\nu/kT_{ex}}-1\right)\right] \end{aligned} \tag{7}$$

T_{ex} is the average excitation temperature along the line of sight; Z the partition function. The molecule has a number density N_0 at r_0 and a spontaneous emission coefficient $A_{J,J-1}$ for the $J \to J-1$ transition at frequency ν. Eq. (6) provides a model for fitting the data with three free parameters: the dimensionless radii r_i/σ and r_e/σ, the tangential optical depth τ_0, and one function, the brightness temperature $T_R(r)$. The latter is assumed to depend simply on a constant average excitation temperature T_{ex}, appropriately corrected for the cosmic background:

$$T_R = \frac{h\nu}{k}\left[\frac{1}{e^{h\nu/kT_{ex}}-1} - \frac{1}{e^{h\nu/kT_{bb}}-1}\right] \tag{8}$$

Our aim is to estimate $N_0 r_0^2$; our strategy is to determine, for each molecular transition, an allowed *range* for the parameters r_e/σ, τ_0 and T_{ex} in several steps:

(1) The fits to the source profile in CO, CS and HCN shown in Figs. 4, 5 & 6 make it possible to guess at a source radius $r_e(mol)$ for each molecular species. We have chosen two prescriptions: the first, giving a 'small' external radius, is to take the half-$T_R(max)$ point of the *deconvolved* profile – for CO this corresponds to assuming that the pointing is accurate for the ^{13}CO spectrum in Fig. 8, giving only a small central dip to this optically thin isotopic line; the second, giving a 'large' external radius, takes twice this value, corresponding to the possibility that the pointing for ^{13}CO may be off by $\sim 5''$. The shape of this line depends sensitively on r_e/σ and therefore, if known, determines this parameter – see step (5) below. There is only a weak dependence on the inner radius r_i provided it is small enough (Olofsson et al. 1982).

(2) We use the line-centre ratio,

$$R_{iso} \equiv \left[\frac{T(main)}{T(isotope)}\right]_{\beta=0} \tag{9}$$

as our second constraint. Assuming the source size is the same in all isotopic variants of a given species, with the same excitation temperature (Olofsson et al. 1982), the overall radiation temperature T_R, Eq. (8), approximately cancels in this ratio. This determines $\tau_0(iso)$, the tangential optical depth of the isotopic species (see Figs. 16–19); the abundance ratio, taken as $[^{12}C]/[^{13}C] \simeq 40$,

Table 2. Observed central temperatures for IRC+10216

Molecule	Transition Frequency(GHz)	Telescope/FWHM	T_A^* (K)	T_R^* (K)	T_{MB} (K)
CO	$J=3-2$ 345.796	NRAO 12m/18″			39.8 ± 2
		JCMT 15m/15″	16 ± 0.8	20 ± 1	37.2 ± 2^a
					29.1 ± 1.5^b
					$(46.7 \pm 2.4)^c$
^{13}CO	$J=3-2$ 330.588	JCMT 15m/15″	1.5 ± 0.1	1.9 ± 0.1	3.5 ± 0.2^a
					2.7 ± 0.2^b
					$(4.4 \pm 0.7)^c$
CO	$J=4-3$ 461.041	JCMT 15m/11″	16.4 ± 0.5		42.0 ± 1.5
CS	$J=7-6$ 342.883	JCMT 15m/15″	5.4 ± 0.4	6.7 ± 0.5	12.5 ± 0.9^a
					9.7 ± 0.7^b
					$(15.8 \pm 2.8)^c$
C^{34}S	$J=7-6$ 337.397	JCMT 15m/15″	0.5 ± 0.05	0.6 ± 0.06	1.2 ± 0.1^a
					0.9 ± 0.1^b
					$(1.5 \pm 0.3)^c$
HCN	$J=3-2$ 265.886	JCMT 15m/23″	17.7 ± 0.5	25.3 ± 0.7	29.5 ± 0.8
H^{13}CN	$J=3-2$ 259.012	JCMT 15m/23″	9.1 ± 0.2	13.0 ± 0.3	15.2 ± 0.3
HCN	$J=4-3$ 354.505	JCMT 15m/15″	29.3 ± 0.8	36.6 ± 1.0	53.3 ± 1.4
H^{13}CN	$J=4-3$ 345.340	JCMT 15m/15″	2.7 ± 0.1	3.4 ± 0.1	4.9 ± 0.2

[a] Based on $\eta_{MB} = 0.43$.
[b] Based on $\eta_{MB} = 0.55$.
[c] Temperatures in brackets are based on requiring consistency with T_{MB} CO $J=3-2$ measured at Kitt Peak. See Sect. 5.

and $[^{32}S]/[^{34}S] \simeq 23$ (Wannier & Linke 1978; Kahane et al. 1988; Sopka et al. 1989), then gives the main species optical depth. It may be that ^{13}CO is radiatively excited (Knapp & Morris 1985), giving a smaller radius and a higher T_{ex}. A smaller radius decreases the integral in eq. (6), compensating for the effect of a higher excitation temperature: the only consequence is to increase the value of our quoted excitation temperature for ^{13}CO by some 20% and the CO abundance by 50%, about the same amount as the difference between the final results quoted in Tables 3 and 4. These tables (and Figs. 16–19) would then be interpreted as tables of ^{12}CO radius and excitation temperature, with ^{13}CO radius about 50% smaller, excitation temperature 20% larger, but with abundances still within the range given there.

(3) The excitation temperature is then determined by fitting the peak temperature of the main line – see Figs. 17–19. Whereas the parameters determined above depend only on dimensionless ratios, T_{ex} depends on the absolute calibration, and is therefore more uncertain. This uncertainty is compounded by the rapid variation of T_{ex} for small values of r_e/σ, which is particularly marked for HCN – Fig. 19 – but is not a problem for the large external radius prescription.

(4) With these values of T_{ex} and τ_0, Eq. (7) enables us to find the shell density $N_0 r_0^2$ – again dependent on the absolute calibration through T_{ex}. The expansion speed V is of course well determined as half the width of the ^{13}CO line – 15.5 ± 1 km/s. The results of this procedure are presented in Table 3.

(5) For CS and HCN these are all the constraints we have, so there is no way of providing an independent check on the recipe used in (1) above for estimating r_e/σ. For CO, however, we can use the *shape* of the ^{13}CO line to provide further independent information as a check on our choice of r_e/σ. In Fig. 16 we show all the constraints in the $\tau_0(13) - (r_e/\sigma)$ plane, where we have described the shape of the ^{13}CO line by two dimensionless parameters: the position of the peak, $\beta = \beta_{max}$, and the ratio of this peak temperature $T(\beta_{max})$ to that at the line-centre, $T(\beta = 0)$, the wing-to-centre contrast: [2]

[2]The approximation given for this ratio by Olofsson et al. (1982), Eq. (2), although adequate for extremely small isotopic optical depths, overestimates C_{iso} for values relevant to this analysis. Thus, for $r_e/\sigma = 1.0$ and $\tau_0 = 0.01$, the approximation yields

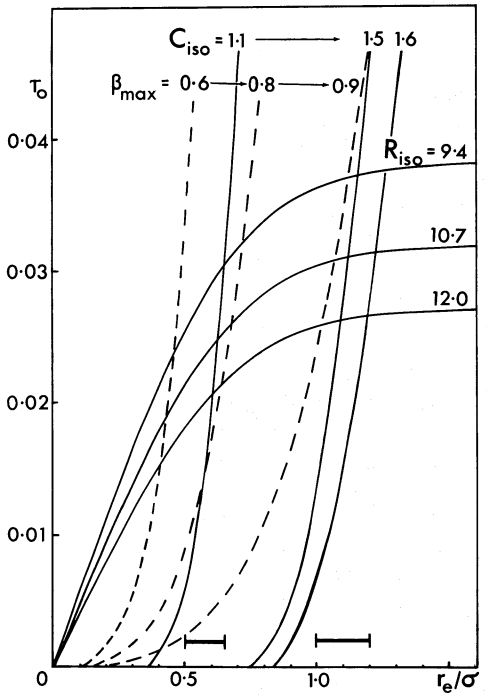

Fig. 16. Dimensionless parameters determining fits to the CO and ^{13}CO $J=3-2$ spectra (Figs.7 & 8) and the CO profile (Fig.4), with vertical axis denoting ^{13}CO tangential optical depth. The profile width is denoted by the horizontal bars for the two alternative prescriptions discussed in the text. The solid curves labelled by $R_{iso} = 10.7 \pm 1.3$ correspond to fixed values for the CO/^{13}CO ratio defined in Eq. (9) and span its likely range of uncertainty. The nearly vertical solid curves span a conservative estimate of the wing-to-centre ratio of the isotopic line, Eq. (10). The dashed curves show the variation of τ_0 with position, β_{max}, of the isotopic peak. We take [^{12}CO]/[^{13}CO]=40

$$C_{iso} = \left[\frac{T(\beta = \beta_{max})}{T(\beta = 0)}\right] \qquad (10)$$

Fig. 16 shows that C_{iso} would strongly constrain r_e/σ if it were known even with moderate accuracy. Assuming the ^{13}CO line of Fig. 8 is exactly on-source we may conservatively estimate $C_{iso} < 1.2$, with $0.6 \leq \beta_{max} \leq 0.8$; this is consistent with a small external radius, $r_e/\sigma \simeq 0.6$. If there is mispointing of 5″ the observed shape of the ^{13}CO line would correspond to an on-source profile with $C_{iso} \simeq 1.6$ and $\beta_{max} > 0.9$; this leads to our second prescription, a large external radius, $r_e/\sigma \simeq 1.1$. We note too that such mispointing would also imply a larger value for the on-source $R_{iso} \simeq 12.0$, at the upper end of the range shown in Figs. 16–17. We emphasize once again that Fig. 16 depends only on dimensionless quantities, and is therefore independent of the absolute calibration. The two alternative prescriptions in (1) above for estimating r_e/σ for CO cover the two extremes in interpreting the ^{13}CO spectrum which makes a realistic allowance for mispointing; and the above discussion provides our justification for using them for CS and HCN. There is an interesting contrast between the two prescriptions, with the lower values of r_e/σ providing a perhaps unreasonably large T_{ex}, especially for HCN $J=4-3$; the higher values give more reasonable excitation

$C_{iso} = 1.9$ compared to the value 1.5 obtained from a full numerical evaluation.

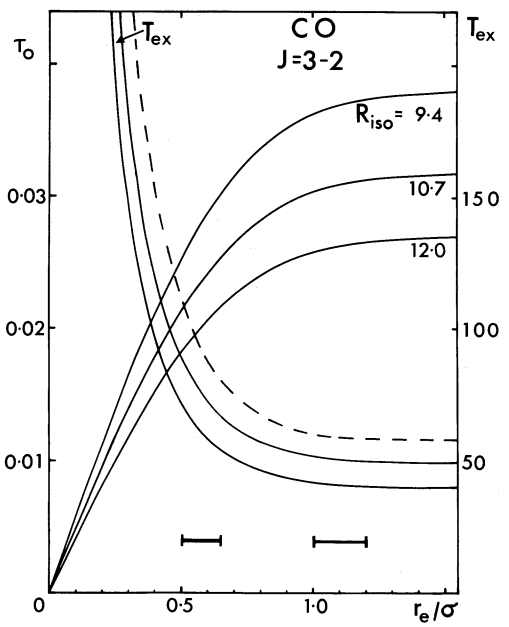

Fig. 17. Dependence of ^{13}CO tangential optical depth, τ_0, and excitation temperature, T_{ex}, on the source/beam ratio r_e/σ for the CO $J=3-2$ transition. Notation the same as Fig.16. The solid T_{ex} curves show the spread for the range of η_{MB} delineated in Table 1 and the range of R_{iso} shown here; the dashed one is the upper limit based on the higher Kitt Peak temperature given in Table 2

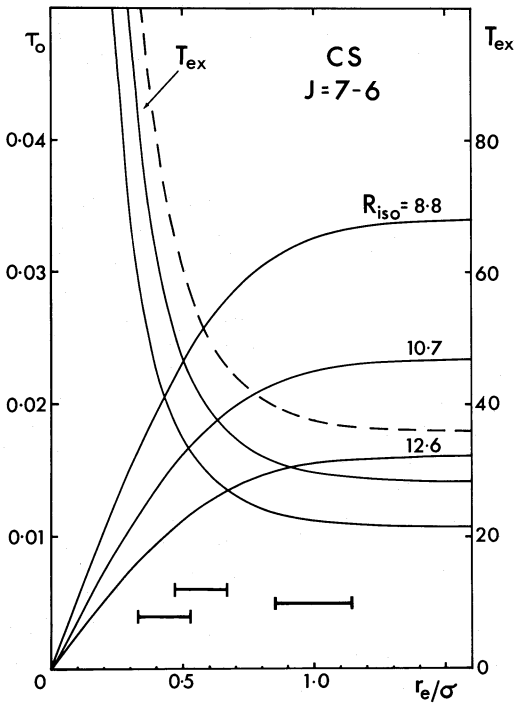

Fig. 18. Dependence of C^{34}S tangential optical depth, τ_0, and excitation temperature, T_{ex}, on the source/beam ratio r_e/σ for the CS $J=7-6$ transition. Notation the same as Figs.16 & 17. The lowest two horizontal bars correspond to the two alternative profile fits in Fig.4; the highest one to the alternative prescription discussed in the text with 'large' radius. We take [C^{32}S]/[C^{34}S]=23

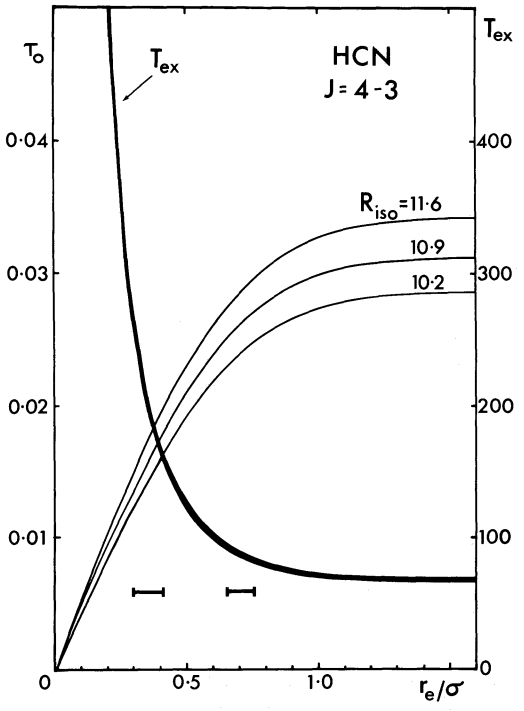

Fig. 19. Dependence of $H^{13}CN$ tangential optical depth, τ_0, and excitation temperature, T_{ex}, on the source/beam ratio r_e/σ for the HCN $J=4-3$ transition. Notation the same as Figs.16 & 17

temperatures rather insensitive to r_e/σ provided it is greater than ~ 0.9. This leads us to favour a large external radius although we have listed both in Tables 3 and 4 where we present the results of the above analysis.

5. Discussion

The [CO]:[HCN] relative abundances obtained in Table 3 are consistent with those obtained from lower frequency observations (Olofsson et al. 1982), while the CS value has not been determined previously. The absolute abundances, which are not in such good agreement, are more sensitive to our simplifying assumptions such as the neglect of IR pumping via vibrational excitation. Another possible source of error is in the calibration of the CO and CS spectra obtained in February, 1988 when Receiver B and the telescope were still quite new. We now consider the possibility that this data may not have been correctly calibrated and look for a comparison with other measurements.

There is only one published measurement of the central temperature for the CO $J=3-2$ line from IRC+10216 (Phillips et al. 1982); none of either CS $J=7-6$ or HCN $J=4-3$. For CO $J=3-2$, there is an unpublished Kitt Peak measurement – quoted by Sahai (1987); revised by Jewell (1989); and confirmed independently at Kitt Peak by Williams et al.(1989) – which is accompanied by an apparently well determined beam efficiency, giving a source centre $T_{MB}= 39.8 \pm 2$ K; the error quoted is our own estimate and does not include uncertainties in the calibration; these may be quite considerable (20–30%) since the CO $J=3-2$ frequency is at the upper limit of the telescope's frequency range where the beam is not well mapped. For the Kitt Peak beam FWHM$\sim$ 18″ this is significantly in excess of the 33 K predicted by the original K-L model and of Sahai's (1987) revised 'standard' model value $\sim$ 25 K; but more in line with the $\sim$ 43 K given by Sahai's (1987) 'best fit' model. It is also in disagreement with our own determination: convolving the K-L profile with the 15″ JCMT beam, but scaled up by the deconvolved Kitt Peak observations, leads to a value T_{MB}=46.7 K, larger by some 17% than the unscaled K-L model and our own measurement. Of course the Kitt Peak, with its wide error beam, cannot be modelled by the single gaussian used in our deconvolution and T_{MB} may not be the appropriate quantity to use for IRC+10216. In that case, in obtaining $T_{MB}=T_R^*/\eta_{MB}$, the correction factor η_{MB} would underestimate the true coupling to an extended source such as IRC+10216 by leaving out the error beam contribution. Thus the true correction factor should be larger with a consequent reduction in the temperature, thus improving agreement with the JCMT value.

On the other hand since our CO $J=3$–2 and CS $J=7$–6 data came from the early operation (February, 1988) of Receiver B a sceptic may question either the calibration, the beam efficiency or both. Suppose we take the extreme position that the correct JCMT $J=3-2$ CO value is as high as T_{MB}=46.7 $\pm$ 2.4 K. This translates into a conversion factor of 2.9 $\pm$ 0.3 on T_A^*, where we have compounded the errors on both the Kitt Peak measurement and our own measurement of T_A^*; this factor of 2.9 is then applied to all the February 1988 Receiver B T_A^* values: CO $J=3$–2, CS $J=7-6$, and their isotopes, but not to the HCN data which was obtained in July 1988. The results are given in Table 2, representing an alternative view of the submillimetre emission from IRC+10216, and the effect on the relative abundances is given in Table 4. Comparing Tables 3 and 4 we note that the abundances and excitation temperatures are all compatible in view of the large uncertainties. These tables probably cover a range of possibilities encompassing all of the main uncertainties: receiver efficiencies and beam shapes, sideband gain ratios, calibrations and atmospheric transmission variations. A representative set of values, assuming there is some mispointing in the ^{13}CO spectrum, is:

$$[CO]:[CS]:[HCN] \simeq 1\times10^{35} : 3\times10^{32} : 1\times10^{35}\ cm^{-1}$$
$$\simeq 1 : 3\times10^{-3} : 3\times10^{-3}$$

with respective excitation temperatures 65, 35 and 90 K.

6. Conclusions

The strengths of the HCN lines and the narrow source profile obtained in HCN $J=4-3$ are consistent with the dominance of radiative excitation for this high dipole moment species. Failure to observe the $C^{18}O$ $J=3-2$ line is consistent with the small ^{18}O abundance for IRC+10216 obtained by Wannier & Linke (1976), $[^{18}O]/[^{16}O] < 4\times10^{-4}$. Similarly, the upper limit obtained for the CI $^3P_1$–$^3P_0$ line can be used to obtain a 1 σ limit on the column density, $N(CI) < 3\times10^{16}$ cm^{-2}, assuming a thermalised, optically thin line and an excitation temperature lying between 20 K and 150 K. Choosing $r_0 = 10^{17}$ cm gives a shell density $N_0 r_0^2 < 3\times10^{33}$ cm^{-1} corresponding to an abundance limit $[CI]/[CO] < 0.03$. Neutral atomic carbon is interesting because it is one of those species predicted to lie in a shell, peaking at a radius of 10^{17} cm (Nejad & Millar 1987). A beam as narrow as 10″will only sample inside this radius, giving an average abundance ratio $[CI]/[CO] < 10^{-3}$ consistent with the observed upper limit. At the same time we note that the existing data on IRC+10216, although extensive, is also lacking in consistency, particularly at higher frequencies. Considerably more careful oversampled mapping is needed, over

Table 3. Model parameters[a]

Mol.	Transition	R_{iso}	r_e	$\tau_0(iso)$	T_{ex} (K)	$N_0 r_0^2$ cm^{-1}	Relative Abundance
CO	$J=3-2$	10.7 ± 1.3	8″	0.025 ± 0.006	71 ± 17	$(0.9 \pm 0.3) \times 10^{35}$	1
			17″	0.031 ± 0.006	45 ± 5	$(0.5 \pm 0.2) \times 10^{35}$	1
CS	$J=7-6$	10.7 ± 1.9	8″	0.018 ± 0.008	37 ± 9	$(3.0 \pm 1.0) \times 10^{32}$	$(3.3 \pm 2.2) \times 10^{-3}$
			6″	0.015 ± 0.008	57 ± 25	$(2.9 \pm 0.9) \times 10^{32}$	$(3.2 \pm 2.1) \times 10^{-3}$
			15″	0.022 ± 0.008	26 ± 4	$(3.5 \pm 1.4) \times 10^{32}$	$(6.5 \pm 4.4) \times 10^{-3}$
HCN	$J=4-3$	10.9 ± 0.7	5″	0.016 ± 0.004	220 ± 50	$(8.1 \pm 2.5) \times 10^{32}$	$(9 \pm 5) \times 10^{-3}$
			11″	0.026 ± 0.002	90 ± 10	$(3.0 \pm 0.7) \times 10^{32}$	$(5.6 \pm 2.9) \times 10^{-3}$

[a] Parameters based on the range $\eta_{MB} = 0.43 - 0.55$ for the r_e prescriptions discussed in the text. Isotopic abundances from Wannier & Linke 1978: $[^{12}C]/[^{13}C]=40$ and $[^{32}S]/[^{34}S]=23$.

Table 4. Alternative model parameters[a]

Mol.	Transition	R_{iso}	r_e	$\tau_0(iso)$	T_{ex} (K)	$N_0 r_0^2$ cm^{-1}	Relative Abundance
CO	$J=3-2$	10.7 ± 1.3	8″	0.016 ± 0.008	97 ± 20	$(1.5 \pm 0.5) \times 10^{35}$	1
			17″	0.031 ± 0.006	63 ± 2	$(1.0 \pm 0.2) \times 10^{35}$	1
CS	$J=7-6$	10.7 ± 1.9	8″	0.019 ± 0.009	51 ± 20	$(3.3 \pm 1.2) \times 10^{32}$	$(2.2 \pm 1.5) \times 10^{-3}$
			6″	0.016 ± 0.008	81 ± 44	$(3.9 \pm 1.7) \times 10^{32}$	$(2.6 \pm 2.0) \times 10^{-3}$
			15″	0.022 ± 0.008	35 ± 3	$(3.2 \pm 1.2) \times 10^{32}$	$(3.3 \pm 2.0) \times 10^{-3}$
HCN	$J=4-3$	10.9 ± 0.7	5″	0.016 ± 0.004	220 ± 50	$(8.1 \pm 2.5) \times 10^{32}$	$(5.4 \pm 3.5) \times 10^{-3}$
			11″	0.026 ± 0.002	90 ± 10	$(3.0 \pm 0.7) \times 10^{32}$	$(3.1 \pm 1.5) \times 10^{-3}$

[a] Parameters based on normalising CO $J=3-2$ to the Kitt Peak value for the r_e prescriptions discussed in the text.

a range of excitation regimes and covering several molecular species and their isotopes. The models also require extension to a range of molecular species besides CO, particularly HCN which is both difficult to treat because of its hyperfine transitions and of great importance because of its strong emission. CS, with a dipole moment midway between those of CO and HCN is a particularly useful diagnostic of the onset of radiative excitation dominance; with better signal-to-noise than we have achieved it would provide excellent constraints on model parameters.

Acknowledgements. We would like to thank the operators and research staff working at the JCMT for their efforts in making these observations possible. We also thank the following for their helpful advice: Richard Hills, Anthony Lasenby, Nick Parker, John Kwan who also provided an updated fit to the CO $J=3-2$ profile, and Rachael Padman for obtaining the CO $J=4-3$ spectrum and allowing us to publish it; thanks finally to our referee, Dr. Forveille, for his helpful suggestions.

References

Becklin, E.E., Frogel, J.A., Hyland, A.R., Kristian, J., Neugebauer, G. 1969, ApJ, 158, L133
Bieging, J.H., Chapman, B., Welch, W.J. 1984, ApJ, 285, 656
Bieging, J.H., Nguyen-Quang-Rieu 1988, ApJ, 329, L107
Bloemhof, E.E., Danchi, W.C., Townes, C.H., McLaren, R.A. 1988, ApJ, 333, 300
Foy, R., Chelli, A., Sibille, F., Lena, P. 1979, A&A, 79, L5
Glassgold, A.E., Lucas, R., Omont, A. 1986, ApJ, 157, 35
Herbig, G., Zappala 1970, ApJ, 162, L15
Huggins, P.J., Glassgold, A.E. 1982, ApJ, 252, 201
Huggins, P.J., Healy, A.P. 1986, ApJ, 304, 418
Huggins, P.J., Olofsson, H., Johansson, L.E.B. 1988, ApJ, 332, 1009
Jewell, P.R. 1989, private communication.
Kahane, C., Gomez-Gonzalez, J., Cernicharo, J., Guelin, M. 1988, A&A190, 167
Knapp, G.R., Morris, M. 1985, ApJ, 292, 640
Kuiper, T.B.H., Knapp, G.R., Knapp, S.L., Brown, R.L. 1976, ApJ, 204, 408
Kwan, J., Hill, F. 1977, ApJ, 215, 781
Kwan, J., Linke, R.A. 1982, ApJ, 254, 587
Lafont, S., Lucas, R., Omont, A. 1982, A&A, 106, 201
Le Bertre, T. 1988, A&A, 203, 85
Lucas, R., Cernicharo, J. 1989, A&A, 218, L20
McCarthy, D.W., Howell, R., Low, F.J. 1980, ApJ, 235, L27
McCabe, E.M., Connon Smith, R., Clegg, R.E.S. 1979, Nature, 281, 263

Mauersberger, R., Guélin, M., Martin-Pintado, j., Thum, C., Cernicharo, J.,Hein, H., Navarro, S. 1989, A&AS, 79, 217
Mamon, G.A., Glassgold, A.E., Huggins, P.J. 1988, ApJ, 328, 797
Martin, P.G., Rogers, C. 1987, ApJ, 322, 374
Miller, J.S. 1970, ApJ, 161, L95
Morris, M. 1975, ApJ197, 603
Morris, M., Alcock, C. 1977, ApJ, 218, 687
Morris, M. 1980, ApJ, 236, 823
Morris, M., Lucas, R., Omont, A. 1985, A&A, 142, 107
Nejad, L.A.M., Millar, T.J. 1987, A&A, 183, 279
Nejad, L.A.M., Millar, T.J. 1988, MNRAS, 230, 79
Nercessian, E., Guilloteau, S., Omont, A., Benayoun, J.J. 1989, A&A, 210, 225
Neugebauer, G., Leighton, R.B. 1969, Two micron sky survey, NASA SP-3047,
Nguyen-Q-Rieu, Bujarrabal, V., Olofsson, H., Johansson, L.E.B., Turner, B.E. 1984, ApJ, 286, 276
Nguyen-Q-Rieu, Epchtein, N., Truong-Bach, Cohen, M., 1987, A&A, 180, 117
Olofsson, H. 1988, Sp.Sci.Rev., 47, 145
Olofsson, H., Johansson, L.E.B., Hjalmarson, A., Nguyen-Quang-Rieu 1982, A&A, 107, 128
Orofino, V., Colangeli, L., Bussoletti, E., Blanco, A., Fonti, S. 1990, A&A, 231, 105
Phillips, J.P., White, G.J., Ade, P.A.R., Cunningham, C.T., Richardson, K.J., Robson, I.E., Watt, G.D. 1982, A&A, 116, 130
Rowan-Robinson, M., Lock, T.D., Walker, W., Harris, S. 1986, MNRAS, 222, 273
Sahai, R., Wannier, P.G. 1985, ApJ, 299, 424
Sahai, R. 1987, ApJ, 318, 809
Sahai, R., van der Veen, W., Stutzki, J. 1990, in preparation.
Sopka, R.J., Olofsson, H., Johansson, L.E.B., Nguyen-Quang-Rieu 1989, A&A, 210, 78
Suttton, E.C., Betz, A.L., Storey, J.W, Spears, D.L. 1979, ApJ, 230, L105
Tamura, M, Hasegawa, T., Ukita, N., Gatley, I., McClean, I.S., Burton, M.G., Rayner, J.T., McCaughrean, M.J. 1988, ApJ, 326, L17
Toombs, R.I., Becklin, E.E., Frogel, J.A., Law, S.K., Porter, F.C., Westphal, J.A. 1972, ApJ, 173, L71
Truong-Bach, Nguyen-Quang-Rieu, Omont, A., Olofsson, H. 1987, A&A, 176, 285
Truong-Bach, Nguyen-Q-Rieu 1989, A&A, 214, 267
Wannier, P.G., Linke, R.A. 1978, ApJ, 225, 130
Williams, P.G., Mampaso, A., Phillips, J.P. 1989, unpublished CO $J = 3 - 2$ Kitt Peak observations.
Williams, P.G., Phillips, J.P. 1990, unpublished Nordic Optical Telescope observations.
Zuckerman, B. 1986, ApJ, 304, 394
Zuckerman, B., Dyck, H.M. 1986, ApJ, 311, 345

This article was processed by the author using Springer-Verlag LaTeX A&A style file 1990.